Direct continuities between cisternae at different levels of the Golgi complex in glucose-stimulated mouse islet beta cells

Brad J. Marsh*†, Niels Volkmann‡, J. Richard McIntosh*, and Kathryn E. Howell§

*Boulder Laboratory for 3D Electron Microscopy of Cells, Department of Molecular, Cellular, and Developmental Biology, University of Colorado, Boulder, CO 80309; ‡The Burnham Institute, 10901 North Torrey Pines Road, La Jolla, CA 92037; and §Department of Cellular and Structural Biology, University of Colorado Health Sciences Center, University of Colorado School of Medicine, Denver, CO 80262

Communicated by Pamela J. Bjorkman, California Institute of Technology, Pasadena, CA, February 23, 2004 (received for review January 10, 2004)

Direct continuity between the membranes of cisternae in the Golgi complex in mammalian cells rarely has been observed; when seen, its documentation has been equivocal. Here we have used dual-axis electron microscope tomography to examine the architecture of the Golgi in three dimensions at ≈6-nm resolution in rapidly frozen, freeze-substituted murine cells that make and secrete insulin in response to glucose challenge. Our data show three types of direct connections between Golgi cisternae that are normally distinct from one another. These connections all "bypass" interceding cisternae. We propose that when pancreatic beta cells are stimulated to synthesize and secrete insulin rapidly *in vivo*, such connections provide a continuous lumen that facilitates the rapid transit of large amounts of newly made protein for secretion. The heterotypic fusion of cisternae, even transiently, raises important questions about the molecular mechanisms that (*i*) facilitate the fusion/fission of cisternal membranes and control the directionality and specificity of such events, and (*ii*) retain Golgi processing enzymes at specific places within individual cisternae when two cisternae at different levels in the Golgi have fused, maintaining the sequential processing hierarchy that is a hallmark of Golgi organization.

The mechanisms by which proteins and lipids move through the Golgi complex remain controversial. There are three prevailing theories for how membrane and luminal cargo are transported: (*i*) by carrier vesicles that move cargo between physically distinct Golgi cisternae in both the anterograde and retrograde directions (1, 2), (*ii*) by the forward movement or "progression" of the cisternae themselves, accompanied by vesicle movement in the retrograde direction (3–5), or (*iii*) by both mechanisms acting in concert (6–8). Direct membrane connections between cisternae at different levels of the Golgi also have been proposed (8–11). Lippincott-Schwartz and colleagues (11) have suggested that such connections might constitute a major mechanism for transport through the Golgi stack, based on data that show first order kinetics for the rate of transport of exogenous viral glycoprotein of vesicular stomatitis virus through the Golgi following its overexpression in cultured cells. Convincing evidence for direct continuity between non-equivalent cisternae has been limited or lacking, although connectivity between cisternae at equivalent levels of the Golgi ribbon is well documented (12–14).

In this study, rapid freezing followed by freeze-substitution fixation of endocrine tissue isolated from mouse pancreas, together with techniques for analyzing electron microscope (EM) data in 3D at ≈6-nm resolution (15), have allowed us to capture and visualize such events in "professional" secretory cells stimulated to make and secrete large amounts of protein. Our observations of membrane trafficking in primary cells maintained in organ culture and stimulated to secrete at high levels suggest that the overexpression of proteins from transgenes in cultured cells lines (11) may be a useful model for biological systems where rates of secretion are naturally high. Thus, the presence or absence of cisternal continuity, previously thought to reflect differences in experimental technique, may in fact represent different states adopted by the cells' secretory machinery as a function of different levels of protein synthesis and transport.

Materials and Methods

Islet Isolation and Culture. Intact islets of Langerhans obtained from the pancreata of freshly killed adult, female, BALB/c mice, were used to ensure that neither cellular polarity nor extracellular matrices were disrupted. Islets were isolated by treatment with collagenase (Sigma type V, lot tested) by means of intraductal injection, and were purified with a Histopaque-1119 density gradient (Sigma) (16, 17). Islets were hand-picked to minimize contamination by residual acinar tissue then cultured in RPMI medium 1640 containing 10% (vol/vol) heat-inactivated FBS and 7 mM D-glucose equilibrated with 5% CO_2 at 37°C. The medium was supplemented with 100 units/ml penicillin/100 μg/ml streptomycin/L-glutamine/2-mercaptoethanol. After culture for 2–3 h, which allowed the isolated tissue to recover, islets were transferred to medium containing low glucose (3 mM) and cultured overnight. This step shifts the beta cell population to basal levels of insulin synthesis and secretion before experimental treatment. Islet beta cells were then stimulated for 60 ± 15 min with 11 mM D-glucose before freezing. Islets were not cultured or used beyond 48 h.

High-Pressure Freezing and Freeze Substitution. Before freezing, islet cultures were kept warm on a humidified heating block at 37°C. The culture medium was buffered by the addition of Hepes (10 mM). The sample holders used for high-pressure freezing experiments [small, brass, sandwich devices comprised of two, interlocking halves ("planchettes")] were also prewarmed to 37°C. Ten to 30 islets (depending on size) were gently manipulated into one half of the holder prefilled with Hepes-buffered RPMI medium 1640 containing FBS 10% (vol/vol) (Sigma). All manipulations were carried out on Parafilm placed on top of an inverted heating block warmed to 37°C under a dissecting microscope. The second half of the planchette, filled with RPMI medium 1640 containing 10% dialyzed Ficoll (molecular mass of 70 kDa) and 0.5% Type IX ultra-low temperature gelling agarose (Sigma) as extracellular cryoprotectants, was then placed on top of the half of the sample holder containing the islets. Islets were frozen within ≈10 msec under high pressure ≈2,100 atm (1 atm = 101.3 kPa)] by using a Balzers HPM 010 high-pressure freezer (BAL-TEC, Balzers, Liechtenstein) and stored under

Abbreviation: EM, electron microscope.

†To whom correspondence should be addressed at the present address: Institute for Molecular Bioscience, Queensland Bioscience Precinct, University of Queensland, Brisbane, QLD 4072, Australia. E-mail: b.marsh@imb.uq.edu.au.

liquid nitrogen. Specimens were freeze-substituted and plastic-embedded essentially as described (15).

Microtomy and Microscopy. Thin (40–60 nm) and thick (300–400 nm) sections cut with a Leica UltraCut-UCT microtome (Leica, Deerfield, IL) were collected onto Formvar-coated copper slot grids. Thin sections were surveyed on a conventional EM operating at 80–120 keV to assess the quality of islet preservation and to select beta cells within the islets for subsequent study. Ribbons of serial thick sections were cut and poststained with 2% aqueous uranyl acetate and Reynold's lead citrate, and were lightly carbon-coated to minimize charging in the EM. Colloidal gold particles (10 or 15 nm) were deposited on both surfaces of these sections for use as fiducial markers during subsequent image alignment. Sections 300–400 nm thick were imaged at 12,000× with a JEM-1000 high voltage EM operating at 750 keV (JEOL). "Tilt series" were digitally recorded with semiautomated methods for charge-coupled device image montaging, data acquisition, and image alignment as the sample was serially tilted at 1.5° angular increments over a range of 120° (±60°) about two orthogonal axes with the microscope control program SERIALEM (18). The 3D density distributions (tomograms) calculated from each set of aligned tilts were aligned with each other and combined to produce a single, dual-axis 3D reconstruction measuring $4.07 \times 4.07 \times 0.4\ \mu m^3$. Subcellular structures and membranes within the 3D volumes were segmented, extracted, and viewed with the IMOD software package (19). For reference, sections cut from plastic (epon) resin are known to collapse by ≈40% in the EM (20). Therefore, a 2.3-nm-thick tomographic slice parallel to the plane of section corresponds to ≈3.9 nm of the specimen before the section collapse that occurs on initial beam exposure. To try to more accurately represent the topology of the structures in the original 400-nm-thick plastic section before imaging in the EM, the 3D model data were stretched by a factor of 1.7 in the *z* axis (15). Algorithms for iterative denoising and semiautomated segmentation of 3D EM data were also used (21).

Online Supporting Information. Fig. 4, which is published as supporting information on the PNAS web site, highlights some of the advanced tools for 3D cell structure analysis that helped us to verify connections between Golgi cisternae in glucose-stimulated beta cells. Movies 1–4, which are published as supporting information on the PNAS web site, show either the 3D tomographic slice data or 3D models incrementally rotated 360° around the *y* and/or *x* axis.

Results and Discussion

The connections between cisternae at different levels of the Golgi were of three types. The first, which has been documented by Rambourg and colleagues (22), occurs at points where the Golgi ribbon branches. The images in Fig. 1 show a branch point where cisternae are connected at both equivalent and nonequivalent levels. In Fig. 1 *A* and *B*, a cisterna from the lower stack (green) is directly continuous with a cisterna at the same level in the upper stack (oriented orthogonally to the lower stack), but is also continuous with a cisterna at a different level. This "Y" configuration of cisternae at the branch in the Golgi ribbon also means that there is direct continuity between cisternae at different levels around the periphery of the upper stack of Golgi membranes (Fig. 1 *B* and *E*). This same type of connection between cisternae at different levels at the periphery of the upper stack was also evident for the alternate cisternae (blue) (Fig. 1 *D* and *F*). The second type of connection occurs when one cisterna projects through an opening (fenestration) in an adjacent cisterna to form a continuous lumen with its next-nearest neighbor (Fig. 1 *C*, *D*, and *F*). Another striking example of this second type of connection between cisternae at different levels, which forms when a cisterna connects to another nonadjacent cisterna through a hole or fenestra, is presented in the images shown in Fig. 2. In the third type of connection, membrane tubules connecting nonequivalent cisternae bypass interceding cisternae at the periphery of the stack in Golgi regions where the ribbon is unbranched (Fig. 3). Although vesicles are present in the Golgi regions of these cells, they have been omitted from the images shown here to allow a better view of the connections between stacked Golgi cisternae. However, discrete vesicles associated with the trans-Golgi (red) can be viewed in Movies 3 and 4.

Even with the advantages provided by the tools for preparation and 3D data analysis used here, the connections we demonstrate are rarely as visually blatant as in Fig. 1, where continuities between cisternae at both equivalent and nonequivalent levels were serendipitously viewed parallel to the plane of section. More frequently, such connections traverse the section obliquely. In the examples of the second and third types of connections provided in the images shown in Figs. 2 and 3, the data were sampled at various orientations in 3D until the membranes of interest could be followed within a single 2D plane and documented unambiguously (Fig. 2 *B* and *C*). Fig. 4 highlights some of the analysis tools that we used for validating such connections between nonequivalent cisternae in 3D following manual segmentation/modeling of the connected membranes. These connections can be followed much more readily in Movies 1–4. Furthermore, it should be noted that the diameters of the connections are typically small (e.g., the connections through fenestrae shown in Figs. 1 and 2 are ≈21 nm in diameter). In the absence of methods for analyzing EM data in 3D at high spatial resolution, and certainly in the case of conventional light microscopy, such connections could not be detected. Even with thin section EM, such connections would at best be difficult to verify but more likely undetectable.

Connections between cisternae at different levels in the Golgi rarely have been observed by conventional EM, even in 3D studies of regulated secretory cells (14, 22), suggesting that these connections are normally short-lived. Such continuities might be even rarer or completely absent in cells not professionally committed to secretion. We propose that these direct continuities are most likely to occur when cells require "high-throughput" anterograde transport through the Golgi, e.g., under conditions where rapid, voluminous protein synthesis and secretion are required because of increased metabolic demand. Such is the case in the present study, where the islet beta cells have been stimulated for 1 h with 11 mM glucose after overnight culture in low (3 mM) glucose-containing medium. Although we have not found such connections in unstimulated cells (data not shown), we cannot rule out the possibility that they exist in the unstimulated state.

Connections that provide a continuous channel between cisternae situated at different levels in the Golgi stack also may help to expedite the retrieval of Golgi-resident membrane proteins and glycosylation/processing enzymes to earlier cisternae in the stack. Such direct connections would theoretically provide a transport mechanism (other than vesicles) that is capable of handling the large volume of retrograde traffic predicted by the cisternal progression-maturation model (23).

Here, we have increased the odds of visualizing such membrane fusion events in two ways. First, rapid freezing has allowed us to capture "snapshots" of rapidly changing physiological states. Even if trafficking events are not stopped instantaneously by this procedure, they must certainly be slowed significantly in the short time (≈10 msec) it takes for the temperature to plummet below −100°C. Second, although it is not possible to synchronize the entire beta cell population within any given islet, we have provoked the beta cells toward maximal proinsulin biosynthesis by shifting them from basal levels of insulin syn-

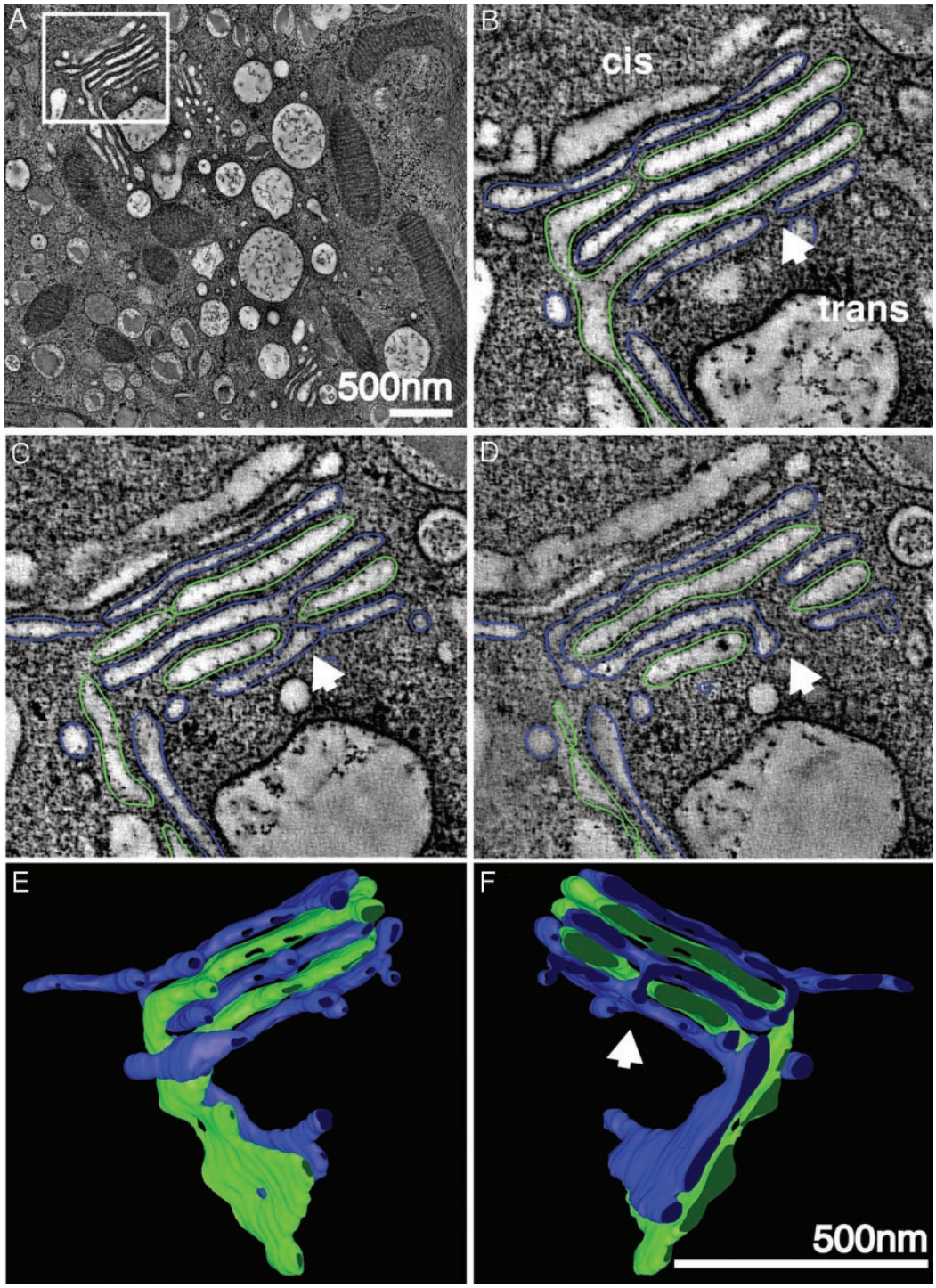

Fig. 1. Cisternal bypass in the Golgi of glucose-stimulated islet beta cells. (*A*) Low magnification overview of the Golgi ribbon in a pancreatic beta cell preserved *in situ* in an isolated mouse islet stimulated with 11 mM glucose for 1 h. The box highlights a branched region of the ribbon shown at higher magnification in *B*, *C*, and *D*. Each panel represents individual (sequential but not adjacent) tomographic slices (z = 2, 9, and 21) extracted from the 103 tomographic slices (each 2.3 nm thick) that together comprise the reconstructed 3D volume. (*B*) The apparent trans-most cisterna (blue) and the penultimate trans-cisterna (green) stay in register where the Golgi ribbon branches. However, all cisternae in the upper stack are not directly continuous across the branch point with cisternae at equivalent levels in the lower stack. Direct continuity between alternating, nonequivalent cisternae (green) occurs laterally at the periphery of a cisternal opening (*A* and *B*). Alternate cisternae (blue) connect directly with each other through an opening or fenestration in the interceding green cisterna (arrowhead). This process is not readily apparent in a single tomographic slice and is thus displayed in two sequential slices that are ≈28 nm apart in the *z* axis (*C* and *D*). (*E* and *F*) Front and back views (rotated 180°) of the 3D model generated by manually segmenting (''modeling'') the tomographic data represented in *A*–*D*. Both types of cisternal bypass can be seen. In *E* and *F*, the lateral continuities at the periphery of the upper stack can be followed; the arrowhead in *F* highlights the connection between cisternae at different levels (blue) through a fenestration or hole in the adjacent (green) cisterna. Movies 1 and 2 that show the original tomographic data (Movie 1), together with the modeled data derived from the 3D reconstructions (Movie 2), allow one to better follow and appreciate these connections. (Scale bars, 500 nm.)

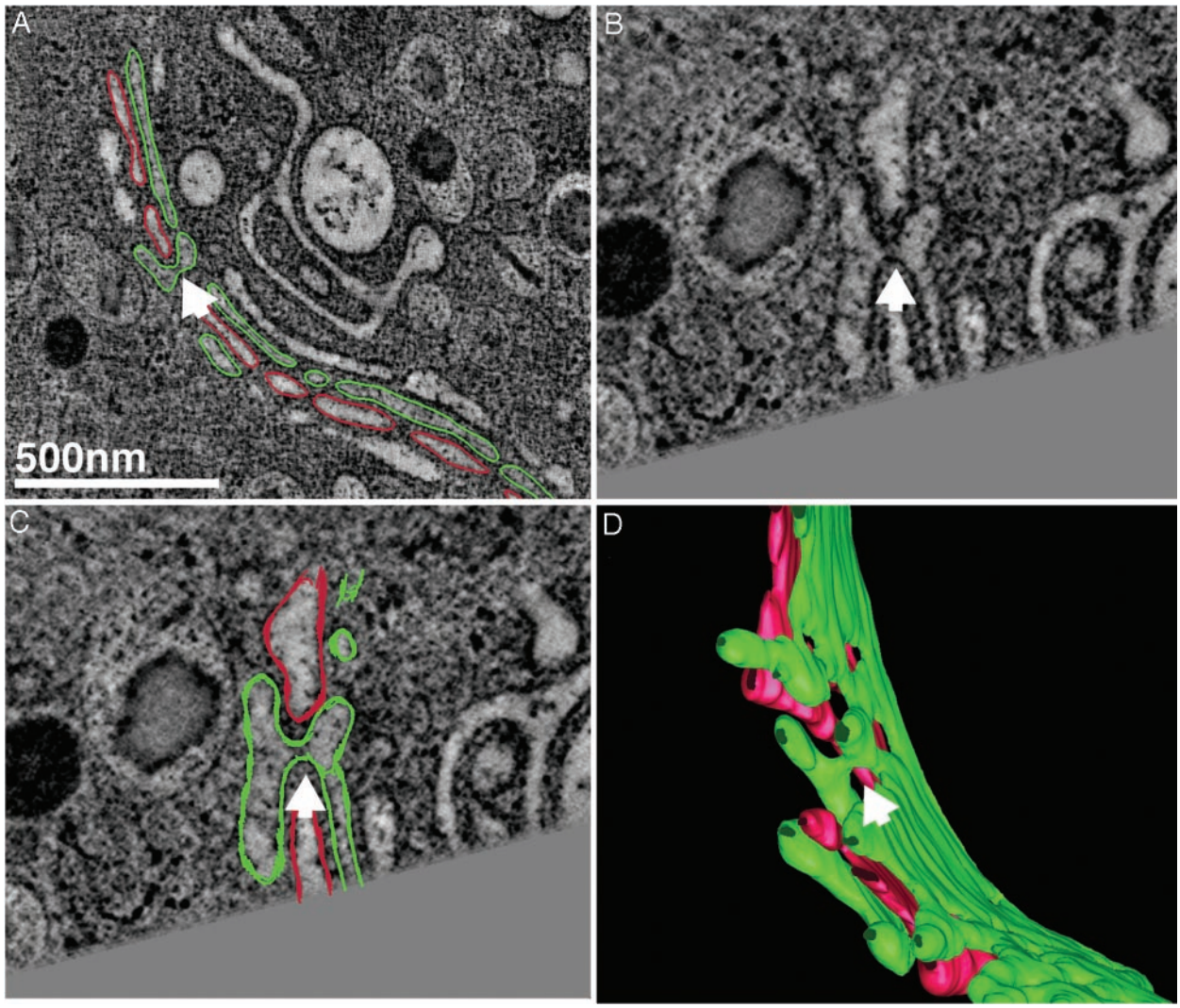

Fig. 2. Cisternal bypass through fenestration of the adjacent cisterna. (*A*) A low-magnification normal *x–y* view of a pixel-thick slice extracted from a 3D reconstruction of a region of the Golgi ribbon from a glucose-stimulated islet beta cell different from that shown in Fig. 1. By using the Slicer tool that is part of the program 3DMOD, we rotated the data by −19.1°, −8.4°, and −32.6° in *x*, *y*, and *z*, respectively, to more clearly visualize the connections both without (*B*) and with (*C*) model contours drawn. The images shown in *B* and *C* each represent the sum of three individual tomographic slices corresponding to a thickness of 6.9 nm. (*C*) Model contours from five tomographic slices are drawn, because the model contours are now oblique to the normal (*x–y*) plane. (*D*) The 3D model generated from the tomographic slice data presented in the preceding panels is shown.

thesis and secretion (3 mM glucose) to high levels (11 mM glucose). This transition from an extended period of "fasting" to high extracellular glucose is accompanied by changes in the surface area and volume of Golgi membranes (24, 25), presumably because of dramatically increased transport of both membrane and luminal cargo through the secretory pathway.

If, as our data suggest, such connections are highly dynamic, then to what extent do membrane proteins and lipids from different cisternae mix? Rothman and colleagues (26) used artificial liposomes to demonstrate that mixing of lumen contents, which takes place during transient soluble *N*-ethylmaleimide-sensitive factor attachment protein receptor-mediated membrane fusion, is accompanied by mixing of the lipid membrane bilayer when fusion occurs at physiological rates. If the connections between nonequivalent cisternae described here facilitate the rapid passage of protein cargo through the Golgi by means of the lumen that forms, it will be important to characterize the molecular machinery that restricts and/or regulates mixing between the membranes of cisternae if they are indeed heterotypic. Further, Nilsson *et al*. (27) showed that the distributions of processing enzymes overlap between medial- and trans-cisternae, and they proposed that Golgi cisternae may be differentiated, not by distinct sets of processing enzymes, but rather by the ratios in which they are mixed. The connections shown here may play a role in regulating the distribution of Golgi enzymes.

It should also be noted that the connections between cisternae at different levels (that extend through fenestrations in Golgi cisternae) that we have observed in these studies is limited to alternating cisternae that are not immediately adjacent. This lack of adjacency is somewhat counterintuitive, because one might expect that if connections between nonequivalent cisternae result from some kind of uncontrolled "blebbing" or fusion event between closely apposed cisternae in the Golgi of glucose-stimulated beta cells after a sustained period of relative inactivity, connections would be more likely to occur (and would require less energy) if they took place between adjacent versus nonadjacent cisternae. Our finding that this does not appear to the case in these studies, together with the paucity of evidence for "vertical integration" within the Golgi by means of mem-

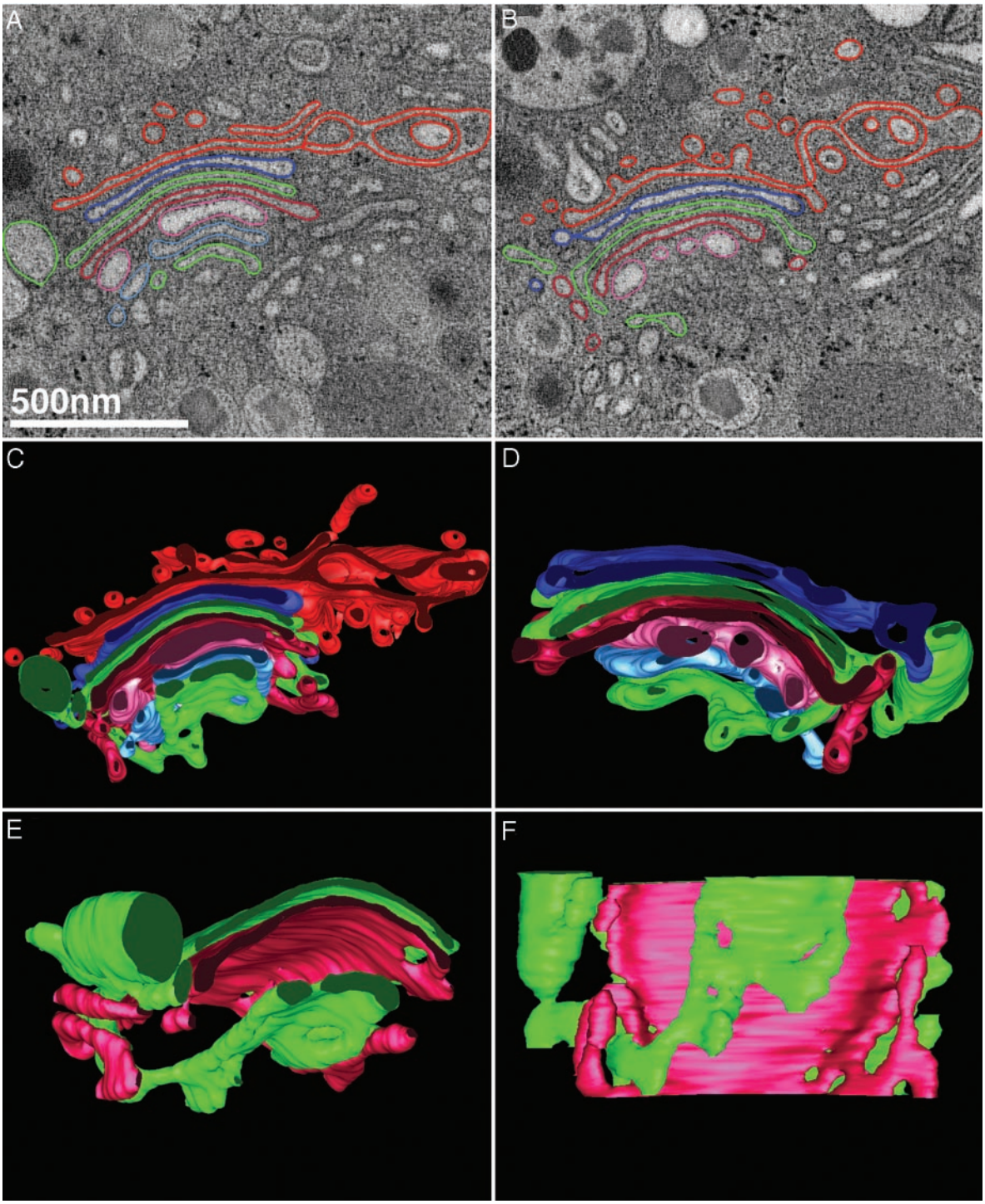

Fig. 3. Cisternal bypass at the stack periphery where the Golgi ribbon is unbranched. An example of the third type of connection between cisternae at different levels in the Golgi of another islet beta cell following glucose-stimulation (60 ± 15 min) is shown. Neither of the two tomographic slices shown in *A* and *B* are able to convincingly demonstrate that the cisternae (green) located at the cis- and trans-sides of the stack (lower and upper faces of the stack, respectively) are directly connected to one another at the periphery of the ribbon. However, when contoured in the *z* axis and rendered in 3D, the tubular membrane lumen connecting each of the flattened, saccular cisternae can be followed in the context of all cisternae within the stack (*C*), including the clathrin-coated trans-most cisterna (red) that presents numerous vesicular and tubular profiles. (*D*) The same stack shown in *C* but viewed from behind (rotated 180°) and without the trans-most cisterna displayed. In *E* and *F*, the connected cisternae (green) are viewed from the front and from below, together with an interceding cisterna (cherry red) for perspective, to allow the reader to visualize the connecting region. In *C* and *D*, it should be noted that none of the cisternae in the Golgi stack are simply ''folded over''; rather, the connection takes the form of a membrane tubule. Movies 3 and 4 of the tomogram of this region shown in *A* and *B* (Movie 3), and of the 3D model data generated by tracing membranes within the reconstructed volume shown in *C–F* allow the interconnected cisternae to be viewed unambiguously as they are rotated around the *x* and *y* axes (Movie 4). Although vesicles are present in the Golgi regions of these cells, we have not shown them for the sake of clarity. However, discrete vesicles associated with the trans-Golgi (red) can be viewed in Movie 4.

brane tubules, suggests that fusion between immediately adjacent cisternae is likely to be directly inhibited, perhaps by the recently identified inhibitory soluble *N*-ethylmaleimide-sensitive factor attachment protein receptors (28).

Although we have convincingly demonstrated the plasticity of individual Golgi cisternae in terms of their capacity to form intercisternal connections in mouse islet beta cells stimulated to make and secrete insulin, we do not know how frequently such connections form or whether they also occur in cells lacking a stimulated, regulated secretory pathway[¶]. It is also noteworthy that there are significant differences between rodent and human islet beta cells at the functional (29–31) and structural levels (32, 33), so it will be important to determine whether such connections also occur in stimulated human islet beta cells.

Our data raise many new questions, not least of which are what mechanisms are at work to induce the formation of these continuities and how the directionality of flow within the lumen is controlled. Answering challenging questions such as these will require us to advance beyond current technology and current thinking about intra-Golgi traffic.

This paper is dedicated to the memory of Barbara Bergman. We thank J. Hutton and B. Bergman for BALB/c islets and reagents, F. Ramirez-Victorino and T. Valentine for islet isolations, and M. Ladinsky and E. O'Toole for helpful discussions. This work was supported by National Institutes of Health Grants GM42629 and P01-GM61306 (to K.E.H.), RR00592 (to J.R.M.), and GM64473 (to N.V.). B.J.M. was supported by Juvenile Diabetes Research Foundation International Postdoctoral Fellowship 3-1999-538.

[¶]Alberto Luini and colleagues have recently observed membrane tubules connecting Golgi cisternae in nocodazole-dissociated Golgi mini-stacks (A. Luini, personal communication).

1. Jamieson, J. D. & Palade, G. E. (1966) *Proc. Natl. Acad. Sci. USA* **55,** 424–431.
2. Rothman, J. E. (1994) *Nature* **372,** 55–63.
3. Grassé, P. P. (1957) *C. R. Acad. Sci.* **245,** 1278–1281.
4. Mollenhauer, H. H. & Whaley, W. G. (1963) *J. Cell Biol.* **17,** 222–225.
5. Bonfanti, L., Mironov, A. A., Jr., Martinez-Menarguez, J. A., Martella, O., Fusella, A., Baldassarre, M., Buccione, R., Geuze, H. J., Mironov, A. A. & Luini, A. (1998) *Cell* **95,** 993–1003.
6. Glick, B. S. & Malhotra, V. (1998) *Cell* **95,** 883–889.
7. Marsh, B. J., Mastronarde, D. N., McIntosh, J. R. & Howell, K. E. (2001) *Biochem. Soc. Trans.* **29,** 461–467.
8. Mironov, A. A., Weidman, P. & Luini, A. (1997) *J. Cell Biol.* **138,** 481–484.
9. Cole, N. B., Smith, C. L., Sciaky, N., Terasaki, M., Edidin, M. & Lippincott-Schwartz, J. (1996) *Science* **273,** 797–801.
10. Weidman, P. J. (1995) *Trends Cell Biol.* **5,** 302–307.
11. Hirschberg, K., Phair, R. D. & Lippincott-Schwartz, J. (2000) *Methods Enzymol.* **327,** 69–89.
12. Rambourg, A. & Clermont, Y. (1990) *Eur. J. Cell Biol.* **51,** 189–200.
13. Ladinsky, M. S., Mastronarde, D. N., McIntosh, J. R., Howell, K. E. & Staehelin, L. A. (1999) *J. Cell Biol.* **144,** 1135–1149.
14. Hermo, L. & Smith, C. E. (1998) *Histochem. Cell Biol.* **109,** 431–447.
15. Marsh, B. J., Mastronarde, D. N., Buttle, K. F., Howell, K. E. & McIntosh, J. R. (2001) *Proc. Natl. Acad. Sci. USA* **98,** 2399–2406.
16. Gotoh, M., Maki, T., Kiyoizumi, T., Satomi, S. & Monaco, A. P. (1985) *Transplantation* **40,** 437–438.
17. Nicolls, M. R., Coulombe, M., Beilke, J., Gelhaus, H. C. & Gill, R. G. (2002) *J. Immunol.* **169,** 4831–4839.
18. Mastronarde, D. N. (2003) *Microsc. Microanal.* **9,** 1182–1183.
19. Kremer, J. R., Mastronarde, D. N. & McIntosh, J. R. (1996) *J. Struct. Biol.* **116,** 71–76.
20. Luther, P. K., Lawrence, M. C. & Crowther, R. A. (1988) *Ultramicroscopy* **24,** 7–18.
21. Volkmann, N. (2002) *J. Struct. Biol.* **138,** 123–129.
22. Rambourg, A. & Clermont, Y. (1997) in *The Golgi Apparatus.*, eds. Berger, E. G. & Roth, J. (Birkhauser, Basel), pp. 37–61.
23. Sannerud, R., Saraste, J. & Goud, B. (2003) *Curr. Opin. Cell Biol.* **15,** 438–445.
24. Boquist, L. & Lorentzon, R. (1979) *Virchows Arch. B. Cell Pathol. Incl. Mol. Pathol.* **31,** 235–241.
25. Perrier-Barta, H. (1984) *Cell Tissue Res.* **237,** 169–179.
26. Nickel, W., Weber, T., McNew, J. A., Parlati, F., Sollner, T. H. & Rothman, J. E. (1999) *Proc. Natl. Acad. Sci. USA* **96,** 12571–12576.
27. Nilsson, T., Pypaert, M., Hoe, M. H., Slusarewicz, P., Berger, E. G. & Warren, G. (1993) *J. Cell Biol.* **120,** 5–13.
28. Varlamov, O., Volchuk, A., Rahimian, V., Doege, C. A., Paumet, F., Eng, W. S., Arango, N., Parlati, F., Ravazzola, M., Orci, L., *et al*. (2003) *J. Cell Biol.* **29,** 79–88.
29. Leiter, E. H. (2002) *Diabetologia* **45,** 296–308.
30. Tyrberg, B., Andersson, A. & Borg, L. A. (2001) *Gen. Comp. Endocrinol.* **122,** 238–251.
31. Petersen, J. S., Russel, S., Marshall, M. O., Kofod, H., Buschard, K., Cambon, N., Karlsen, A. E., Boel, E., Hagopian, W. A., Hejnaes, K. R., *et al*. (1993) *Diabetes* **42,** 484–495.
32. Brelje, T. C., Scharp, D. W. & Sorenson, R. L. (1989) *Diabetes* **38,** 808–814.
33. Hagopian, W. A., Karlsen, A. E., Petersen, J. S., Teague, J., Gervassi, A., Jiang, J., Fujimoto, W. & Lernmark, A. (1993) *Endocrinology* **132,** 2674–2681.
34. Yang, G. J. & Huang, T. S. (1981) *Comput. Graphics Image Proc.* **15,** 224–245.